Please cite this article in press as: Broz et al., Dissecting the Tumor Myeloid Compartment Reveals Rare Activating Antigen-Presenting Cells Critical for T Cell Immunity, Cancer Cell (2014), http://dx.doi.org/10.1016/j.ccell.2014.09.007

Cancer Cell
Article

Dissecting the Tumor Myeloid Compartment Reveals Rare Activating Antigen-Presenting Cells Critical for T Cell Immunity

Miranda L. Broz,[1] Mikhail Binnewies,[1] Bijan Boldajipour,[1] Amanda E. Nelson,[1] Joshua L. Pollack,[2] David J. Erle,[2] Andrea Barczak,[2] Michael D. Rosenblum,[3] Adil Daud,[4] Diane L. Barber,[5] Sebastian Amigorena,[7] Laura J. van't Veer,[6] Anne I. Sperling,[8] Denise M. Wolf,[6] and Matthew F. Krummel[1,*]
[1]Department of Pathology
[2]Lung Biology Center
[3]Department of Dermatology
[4]Melanoma Clinical Research Unit
[5]Department of Cell and Tissue Biology
[6]Department of Laboratory Medicine
University of California San Francisco, San Francisco, CA 94143, USA
[7]INSERM U932, Immunity and Cancer, Institut Curie, 75248 Paris Cedex 05, France
[8]Committee on Immunology, University of Chicago, 924 E. 57th Street, Chicago, IL 60637, USA
*Correspondence: matthew.krummel@ucsf.edu
http://dx.doi.org/10.1016/j.ccell.2014.09.007

SUMMARY

It is well understood that antigen-presenting cells (APCs) within tumors typically do not maintain cytotoxic T cell (CTL) function, despite engaging them. Across multiple mouse tumor models and human tumor biopsies, we have delineated the intratumoral dendritic cell (DC) populations as distinct from macrophage populations. Within these, CD103$^+$ DCs are extremely sparse and yet remarkably capable CTL stimulators. These are uniquely dependent on IRF8, Zbtb46, and Batf3 transcription factors and are generated by GM-CSF and FTL3L cytokines. Regressing tumors have higher proportions of these cells, T-cell-dependent immune clearance relies on them, and abundance of their transcripts in human tumors correlates with clinical outcome. This cell type presents opportunities for prognostic and therapeutic approaches across multiple cancer types.

INTRODUCTION

In immunoevasive tumors, a complex microenvironment develops alongside the lesion, and despite the recruitment of CD8 T cells, there is no effective control of the developing mass. This microenvironment is prominently composed of the mononuclear phagocytic lineage (MPS) in addition to tumor-associated fibroblasts (TAFs) and a variety of additional immune infiltrates, including neutrophils and tumor-specific T cells (Hanahan and Weinberg, 2011; Kraman et al., 2010). A primary conundrum at present is to understand why the latter cells, which include CD8$^+$ T cells with the potential to kill the tumor, ultimately fail to do so.

The MPS lineage typically should have the potential to present antigens to T cells by virtue of their phagocytic capacity. In tumors, the infiltrating MPS lineage has been described as comprising tumor-associated macrophages (TAMs; see Lewis and Pollard, 2006), tumor dendritic cells (DCs), as well as monocytes. While monocytes do not clearly function as APCs, they may act at minimum as precursors to TAMs and DCs in normal and transformed tissues (Cheong et al., 2010; Cortez-Retamozo et al., 2012; Geissmann et al., 2010). A number of studies have

Significance

Current cancer immunotherapies are based on enhancing the ability of host or introduced T cells to reject tumors. However, efficient CTL function requires frequent repriming and abundant tumor macrophages, which capture CTL at the tumor margin, either fail to achieve this, and/or actively inhibit T cell responses. Here we show that the abundant macrophages in tumors have a functional opposite, in the form of antigen-presenting CD103$^+$ DCs. These cells efficiently cross-present tumor antigens and are differentially distributed within the tumor microenvironment compared with tolerizing APCs. We describe how intratumoral CD103$^+$ DCs are uniquely targetable, how their abundance is required for T cell therapy in mice, and how their transcript prevalence predicts outcome in human cancers.

Please cite this article in press as: Broz et al., Dissecting the Tumor Myeloid Compartment Reveals Rare Activating Antigen-Presenting Cells Critical for T Cell Immunity, Cancer Cell (2014), http://dx.doi.org/10.1016/j.ccell.2014.09.007

implicated specific MPS-lineage-derived cells, particularly immature monocytes, in dampening the responsiveness of cytotoxic T cells (CTLs) in tumors (Kusmartsev et al., 2005). Through intravital imaging, we and others have found that antigen-specific CD8$^+$ T cells are initially captured in prolonged interactions with myeloid cells, along the tumor border (Boissonnas et al., 2013; Engelhardt et al., 2012). In those experiments, the myeloid cells that phagocytosed tumor antigens and cross-presented them, when purified in aggregate, failed to stimulate T cells in vitro. Thus, by all criteria to date, the immune microenvironment is a combination of poorly stimulatory and/or actively inhibitory APC partners for CTLs. While depletion of regulatory T cells and checkpoint blockades are suggested to broadly license tumor APCs (Curran et al., 2010), there has been no evidence of strongly stimulatory APCs within the native tumor.

As immunotherapies targeting costimulatory blockade (Leach et al., 1996) move to the forefront of cancer therapeutics, it becomes increasingly important to understand the spatial and temporal context of costimulation and antigen presentation. Antigen presentation at the lymph node (LN) for priming of tumor-reactive T cell expansion is clearly critical and as such has been successfully targeted therapeutically using GM-CSF (Dranoff, 2002) to increase presentation in the LN. As such, much of the focus has remained on the LN despite our clear understanding that antigen presentation also occurs within the tumor itself and likely influences the functions of tumor CTLs.

It was therefore our goal to dissect the distinct composition of the myeloid tumor microenvironment across a broad range of tumors, with the purpose of understanding the lineage relationships among these populations and how each influenced tumor T cell responses and outcome.

RESULTS

Surface Markers Delineate Rare Tumoral DC Subsets from Abundant Macrophages

To dissect the tumor-infiltrating myeloid populations, we devised an 11-color flow cytometry panel and progressive gating strategy using a spontaneous breast tumor model, PyMTChOVA (Engelhardt et al., 2012), engineered along with the initiating oncogene to independently coexpress fluorescent mCherry protein and ovalbumin. We profiled the tumoral CD45$^+$ compartment, many of which had phagocytosed tumor antigen and thus exhibit mCherry fluorescence (Figure 1A). Subgating all hematopoietic cells by the myeloid-specific marker CD11b and the monocyte marker Ly6C allowed removal of neutrophils and monocytes (see Figure S1A available online). Within the MHCII$^+$ cells, DCs were distinguished from macrophages based on CD24^{hi} and F4/80^{lo} expression, neither of which alone is sufficient to make this distinction. Subsequently, DCs were found to parse into two populations based on differential expression of CD11b and CD103, as has been observed in healthy peripheral tissues (Hashimoto et al., 2011). We found these populations in two mouse models of melanoma (B78ChOVA, a variant of B16 expressing mCherry and OVA, Figure 1B, and BRAF V600E, Figure S1B), across mouse strains (e.g., FVB PyMT; Figure S1B), and in ectopic tumors (Lewis Lung Carcinoma; Figure S1B). We refer to these DC populations as "CD11b$^+$ DC1" and "CD103$^+$ DC2" henceforth for ease of discrimination and discussion.

Parsing of the F4/80^{hi} CD24^{lo} compartment also revealed two types of macrophages, identified by differential expression of CD11c and CD11b. CD11c^{lo} CD11b^{hi} (heretofore "TAM1") and CD11c^{hi} CD11b^{lo} cells ("TAM2") appear to broadly correspond to similarly delineated MHCII^{hi} and MHCII^{lo} populations (Movahedi et al., 2010) (see Figure 5C). While CD11c, otherwise a "prototypical" DC marker, was highest on DCs, it was highly expressed in TAM2 and to a lesser extent in TAM1 (Figure S1C). These populations existed across all models examined, although the prevalence of each and their ability to be unambiguously distinguished varied slightly (Figures 1A, 1B, and S1B). For the rest of this report, we therefore applied our lineage and function studies to one example of spontaneous (PyMTChOVA) and ectopic tumor model (B78ChOVA), except where indicated.

mCherry loading and retention, derived from the tumor, were assessed for each of these populations. This revealed that the uptake^{hi} cells, localized to the tumor margin in our previous report and then identified only by CD11c (Engelhardt et al., 2012), were best captured in the TAM1 and TAM2 gates (Figures 1C and S1D). Comparatively, CD11b$^+$ DC1s and CD103$^+$ DC2s took up or retained less mCherry while some monocytes but few neutrophils showed evidence of modest antigen loading.

CD11b$^+$ and CD103$^+$ DC subsets have been found in many peripheral mouse tissues, and their counterparts have been identified in peripheral human tissues, defined by expression of BDCA1 and BDCA3, respectively (Dzionek et al., 2000; Haniffa et al., 2012). We found that an equivalent TAM/DC distinction was also possible in human metastatic melanoma samples using these markers (Figure 1D). CD16$^-$HLADR$^+$ CD11c$^+$CD14$^+$ cells representing all TAMs were distinct from CD16$^-$HLADR$^+$ CD11c$^+$CD14$^-$ DC populations, which were in turn parsed by differential expression of BDCA1 ("DC1") and BDCA3 ("DC2"). Common across mouse models (Figure 1E) and human melanoma biopsies (Figure 1F) are the presence and rarity of the CD11b$^+$/BDCA1 DC1 and CD103$^+$/BDCA3 DC2 populations, with DC2 being particularly sparse.

Protein and Transcriptional Delineation of Tumor DCs and Macrophages

To validate our gating strategies, we applied panels of antibodies defined by the ImmGen consortium (Gautier et al., 2012; Miller et al., 2012). Consistent with our assignment of "DC," CD103$^+$ DC2 expressed CD135 FTL3 CD117 (cKit), and CD26, whereas both TAM populations did not in the B78chOVA and PyMTchOVA models (Figures 2A and S2A). Surprisingly, CD11b$^+$ DC1 did not express detectable levels of DC markers and actually segregated more with TAM1 and TAM2 by virtue of expression of several "macrophage" markers, including CD206, CD64, and MerTK (Figures 2B and S2B). CD11b$^+$ DC1, however, slightly expressed CD301b and PDL2, both of which have been used to define IRF4-dependent "DC$_{Th}$2" populations found in the skin (Figures 2C and S2C) (Gao et al., 2013; Kumamoto et al., 2013).

To further delineate these APCs, we analyzed the gene expression profiles of sorted cells from B78chOVA tumors using RNAseq. As shown in Figure 2D, blocks of genes clearly segregate the four populations, with TAM1, TAM2, and CD11b$^+$ DC1 being the most similar by PCA analysis (Figure 2E) and CD103$^+$ DC2 the most distinct. Among the genes most differentially

Please cite this article in press as: Broz et al., Dissecting the Tumor Myeloid Compartment Reveals Rare Activating Antigen-Presenting Cells Critical for T Cell Immunity, Cancer Cell (2014), http://dx.doi.org/10.1016/j.ccell.2014.09.007

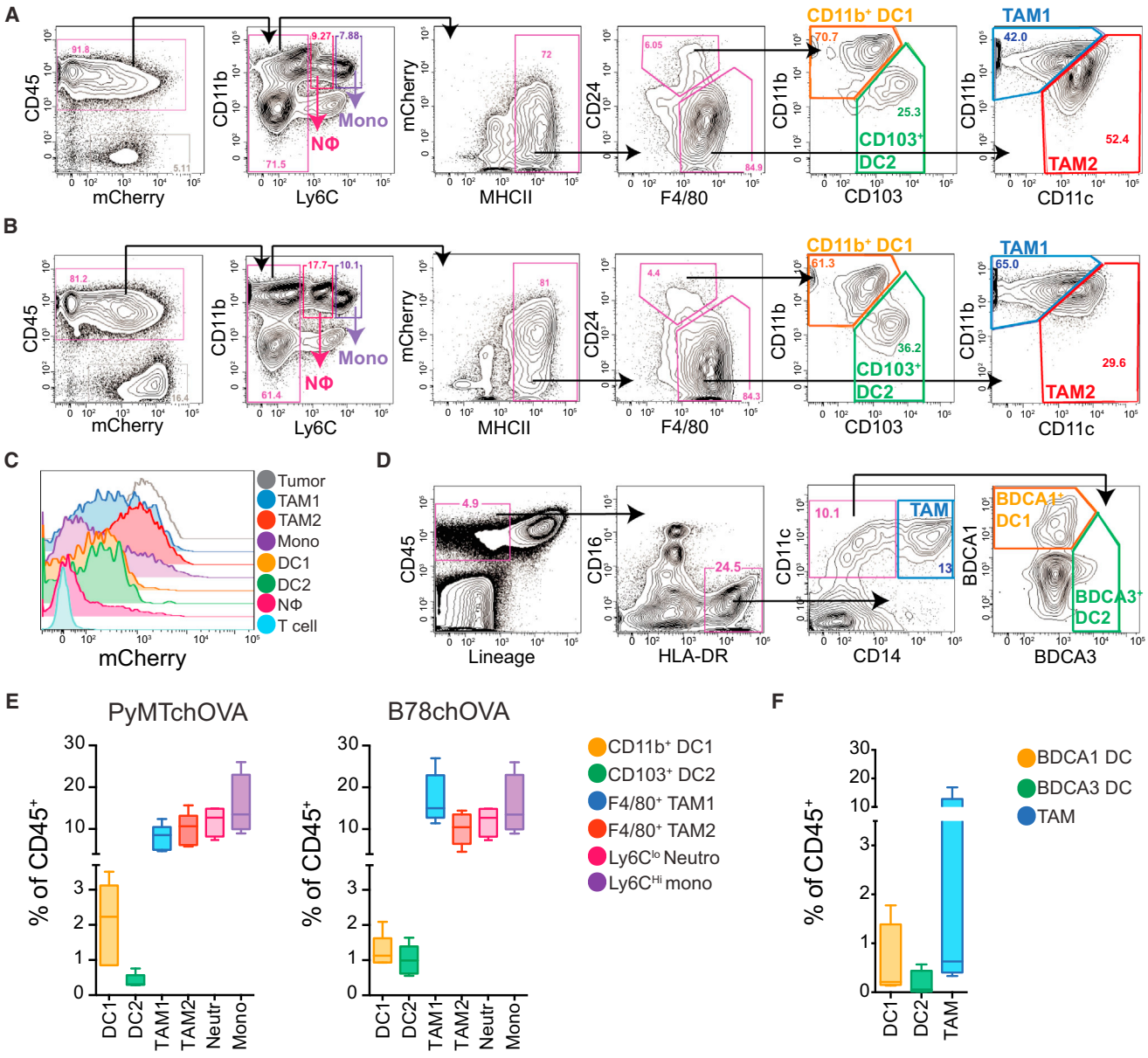

Figure 1. Rare DC and Abundant Macrophages in Mouse and Human Tumors

(A–C) Representative of greater than five independent experiments. (A) Flow cytometry and gating of tumor APC populations from digested and CD45-enriched PyMTchOVA tumors. (B) Cytometry of tumor APC populations in ectopic B78ChOVA tumors. (C) Histogram of tumor-derived mCherry fluorescence by tumor-infiltrating immune cells in B78chOVA.

(D) Representative cytometry of digested human melanoma metastatic biopsy identifying corollary DC and TAM populations defined by CD45⁺ Lin⁻ (CD3e, CD56, CD19) HLA-DR⁺ and split by CD14, BDCA1, and BDCA3. Double-negative cells likely reflect B cells escaping lineage gate, immature monocytes, or pDC.

(E) Relative proportions of tumor infiltrating myeloid cells as a percentage of total CD45⁺ cells for PyMTchOVA and B78chOVA models. Pooled data from individual tumors are presented as mean ± SEM (n = 5) from mice.

(F) Frequency of DC and TAM populations infiltrating human metastatic melanoma presented as a percentage of total CD45⁺ cells. Pooled data from multiple patients are presented as mean ± SEM from (n = 4) biopsies.

See also Figure S1.

expressed, DC lineage-defining transcription factors *Irf8* (Tamura et al., 2005) and *Zbtb46* (zDC) (Meredith et al., 2012) were specific for CD103⁺ DC2 alone, or both DCs, respectively, whereas *Irf4* was modestly enriched in CD11b⁺ DC1 and all of which were validated by quantitative RT-PCR (qRT-PCR) (Figure 2F). This was also confirmed at the protein level by intracellular flow cytometry for IRF4/8 (Figures 2G and S2D). All populations expressed *Myb*, which indicates hematopoietic stem cell origin as opposed to deriving from tissue precursors, seeded from the yolk sac (Schulz et al., 2012).

As these intratumoral populations may derive through distinct tumor-specific mechanisms and not rely on these transcription

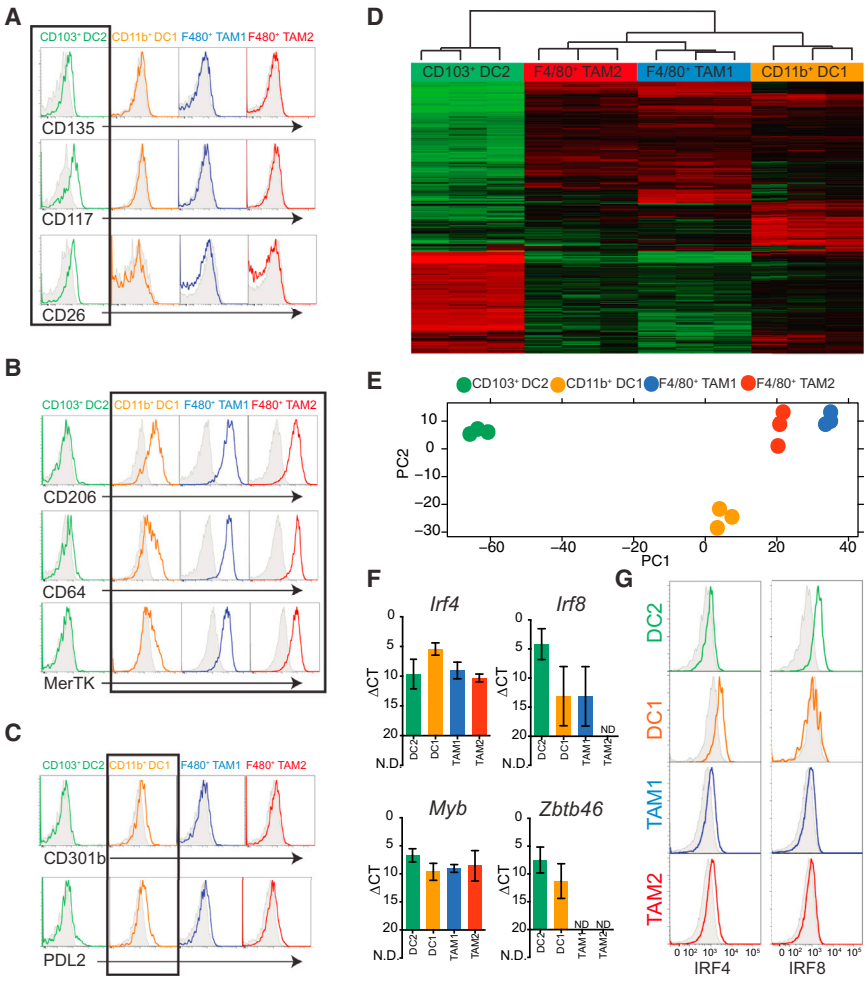

Figure 2. Surface and Transcriptional Profiling Highlights Distinct Lineages of Tumor DCs and Macrophages

(A) Expression of a panel of DC specific markers compared with respective isotype (gray shaded). A black box outlines the CD103$^+$ DC2 population.

(B) Differential expression of Macrophage specific markers (colored) with corresponding isotypes (gray shaded). A black box outlines the CD11b$^+$ DC1, TAM1, and TAM2 populations.

(C) Specific expression of DC-T$_h$2 makers (colored) by CD11b$^+$ DC1 populations compared with respective isotype (gray shaded). A black box outlines CD11b$^+$ DC1.

(D) Global transcriptional profiles revealed by RNAseq of FACS-purified populations from biological triplicates. Data are displayed as a heat map of $\log_2$-fold change relative to the global average of the top 1,000 genes by maximum variance between DC1, DC2, TAM1, and TAM2.

(E) PCA of DC1, DC2, TAM1, and TAM2 populations based on RNAseq global transcriptional profiles.

(F) qRT-PCR analysis of expression of *Irf4*, *Irf8*, *Myb*, and *Zbtb46* (zDC) from sorted APC populations. Data are presented as mean Δ Ct ± SEM calculated from biological triplicates (n = 3) (N.D., not detected).

(G) Intracellular staining for IRF4 and IRF8 in tumor APC populations as compared with the respective isotype (gray).

All data are from the ectopic B78chOVA tumor model. Cell lineages are defined as in Figure 1. See also Figure S2.

factors as they do in some normal tissues, we investigated IRF8, IRF4, Batf3, and zDC dependency using knockout or transcription-factor-driven diphtheria toxin receptor (DTR) mice. We took advantage of various ectopic tumors, due to the vagaries and length of breeding these alleles to a spontaneous model. Using an ectopic PyMT breast tumor model, we found that loss of *Irf8* specifically ablated the CD103$^+$ DC2s but did not affect TAM1 or TAM2 and mildly enriched the percentage of CD11b$^+$ DC1, perhaps as a result of compensation (Figure 3A). Conversely, conditional deletion of *Irf4*, driven by *CD11c*-Cre (Williams et al., 2013), resulted in the specific reduction in CD11b$^+$ DC1 with little change in the others in the B78chOVA model (Figure 3B). In agreement with RNAseq data, *Batf3*-deficient animals also lacked tumoral CD103$^+$ DC2 populations in a B78chOVA model, without effect on CD11b$^+$ DC1, TAM1, or TAM2 proportions (Figure 3C). Finally, when a *zDC*-driven DTR allele was used, we somewhat unexpectedly found a specific and significant reduction in CD103$^+$ DC2 with little or no changes in the CD11b$^+$ DC1 or TAM1/TAM2 populations in B78chOVA tumors (Figure 3D). This may represent vagaries of the DTR allele or subtle but significant variations in *zDC* expression. Taken together, we conclude that CD103$^+$ DC2 represents a distinct lineage of APC as compared with CD11b$^+$ DC1 and the highly abundant TAM1/TAM2 in the tumor.

CD103$^+$ DC2 Are Programmed by Distinct Cytokines

APCs derive from bone marrow (BM) precursors, and their differentiation into DC/macrophage subsets depends on specific cytokines. To determine the cytokines driving differentiation into these populations, we queried colony-stimulating factor (CSF) receptor expression across models by qPCR. Whereas *Csf1r* (M-CSFR) was found exclusively in TAM1, TAM2, and CD11b$^+$ DC1, *Csf2rb* (GM-CSFR) was uniquely expressed in the DC1 and DC2 subsets, and *Csf3r* (G-CSFR) was absent in all (Figure 4A). Using either neutralizing antibody treatment or cytokine-receptor-deficient mice with ectopic tumors, we functionally tested CSF cytokine reliance of the APCs at the tumor.

While TAM1 and TAM2 cells critically relied on CSF1 for their maintenance, as has been shown previously (Wyckoff et al., 2004), CD11b$^+$ DC1 and CD103$^+$ DC2 populations were uniquely independent of CSF1 (Figure 4B). For use of cytokine receptor-deficient mice, we developed a congenic adoptive transfer model, whereby granulocyte macrophage progenitors (GMPs) were transferred into ectopic tumor-bearing hosts and repopulation was tracked in the BM, spleen, and tumor (Figure 4C). At the tumor GMP-derived cells populated all myeloid compartments, confirming GMP origin of CD11b$^+$ DC1, CD103$^+$ DC2, TAM1, and TAM2 (Figure 4D). By use of the GMP adoptive system with a competitive transfer, we found a selective inability of

Csf2rb$^{-/-}$ cells to reconstitute DCs at the tumor, here defined as the sum of DC1/DC2 using CD24$^+$ CD11c$^+$ gating. We found no effect on TAM1 and TAM2 repopulation, suggesting a unique requirement of CSF2 (GM-CSF) for tumoral DC development (Figure 4E) while no requirement for CSF-3 was found for any of the four APCs (Figure S3).

As DCs are prototypically driven by GM-CSF or FLT3-ligand (FLT3L), we assessed cytokine sufficiency to drive DC populations at the tumor using B16 melanoma tumor models engineered to express GMCSF or FLT3L. While GMCSF expression by the tumor drastically skewed the proportion of CD11b$^+$ DC1, FLT3L expressing tumors drove unique expansion of the rare CD103$^+$ DC2 at the tumor (Figure 4F).

Unique Antigen Processing and Presentation Capabilities of CD103$^+$ DC2

Having established the lineage requirements of the different APCs, we then assessed their ability to initiate, engage, and sustain T cell responses. To parse the cells with regard to antigen processing, presentation, and costimulation, we analyzed transcript and protein levels of genes involved in these pathways using RNASeq data from Figure 2. Differences were considerable, across broad swaths of potential APC function (Figure 5A). Notably, while surface levels of molecules involved in regulating T cell responses, including CD80, CD86, and 2B4, were comparable between populations, CD103$^+$ DC2s showed distinct transcriptional signatures consistent with heightened cross-presentation, enhanced costimulation, and increased expression of chemokines that would be expected to enhance T cell interactions (Figures 5A, 5B, and S4A). There were no major differences in MHCI and MHCII expression between the APCs with the exception of slightly reduced MHCI on CD103$^+$ DC2 (Figure 5C). However, significant differences in phagocytic capacity were observed in CD103$^+$ DC2s compared with TAM1/TAM2, measured exogenously by ex vivo dextran uptake from ectopic tumors (Figure 5D).

As DC maturation and phagocytic capacity are often inversely correlated, we hypothesized that the decreased phagocytic capacity of CD103$^+$ DC2 might correspond to a more mature DC with increased cross-presentation of antigen (Guermonprez et al., 2002). Efficient cross-presentation of antigen in DCs relies on NOX2 to regulate phagasomal pH, thereby preventing destruction of T cell peptides, which can be determined using a ratiometric assay comparing intracellular fluorescence intensity of a pH-sensitive and pH-insensitive fluorophore following phagocytosis (Savina et al., 2006). We therefore generated a B78 tumor line expressing a fusion of a pH-sensitive GFP (pHluorin, quenched below pH 6.5) and a pH-insensitive fluorophore (mCherry). By analyzing pHluorin intensity alone within the mCherry$^+$ compartment of each population, we found that only the "DC" populations maintained pHluorin in an alkaline (fluorescent) environment; comparing the ratio of pHluorin and mCherry signals showed that CD103$^+$ DC2 maintained the most basic endocytic compartment, while TAM1 and TAM2 populations displayed highly acidic and therefore degradative phagocytic pathways (Figure 5E). In addition to the increased alkaline phagosomal lumen of CD103$^+$ DC2, these cells demonstrated differential expression of the proinflammatory cytokine interleukin-12 (IL-12) and absence of anti-inflammatory IL-10 (Figures 5F, 5G, and S4B). Together, all of these features suggest CD103$^+$ DC2s are highly poised for efficient antigen cross-presentation to CD8$^+$ T cells.

CD103$^+$ DC2s Are Superior Stimulators of Naive and Activated CD8$^+$ T cells

Previously, we found that the aggregate antigen-ingesting myeloid compartment could stimulate naive but not previously activated CD8$^+$ T cells when taken directly from tumors (Engelhardt et al., 2012). However, based on the unique cross-presentation phenotype of CD103$^+$ DC2, we sought to test the T cell stimulatory capacity of each population, freshly isolated from tumors. After 12 hr of coculture with ovalbumin-specific OT-I CD8$^+$ T cells, the CD103$^+$ DC2 population was the only population capable of robustly inducing TCR signaling, measured by GFP expression driven by a *Nur77* reporter (Nur77^{GFP}) and CD69 levels in both naive and previously activated OT-I CD8$^+$ T cells. Importantly, this was consistent in both ectopic and spontaneous mouse models (Figures 6A and S5A). Extended coculture of dye-labeled OT-I CD8$^+$ T cells revealed that CD11b$^+$ DC1 and CD103$^+$ DC2 populations were the most robust stimulators of naive CD8$^+$ T cell proliferation and demonstrated that nearly the entire stimulatory capacity previously identified in phagocytosing tumor myeloid cells lies within these DC (Figures 6B, 6C, S5B, and S5C). Interestingly, CD103$^+$ DC2 were uniquely capable of inducing strong proliferation of established CTLs, which were not stimulated by the other populations, indicating that CD103$^+$ DC2 were superior cross-presenting stimulators of CTLs in the tumor (Figures 6D, 6E, and S5D, respectively).

Ultimately, at their normally low frequencies in total tumor isolate, CD103$^+$ DC2s remain unable to drive proliferation of CTLs (Figure S5E; Engelhardt et al., 2012). Additionally, none of the APC subsets induced CD4$^+$ T cell proliferation directly from the tumor (Figures 6F, 6G, and S5F). However exogenous peptide did restore DC1 and DC2 capacity to stimulate proliferation, suggesting these DCs may not be inherently incapable of CD4 T cell stimulation (Figure S5G). Critically, this identifies the unique capacity of CD103$^+$ DC2 within the tumor to uptake, process, and cross-present tumor antigen to robustly stimulate CTLs. This challenges the simple concept that tumors contain only weak or suppressive myeloid populations.

CD103$^+$ DC2 Localization and T Cell Interactions Revealed by Intravital Imaging

Given the unique ability of the rare CD103$^+$ DC2s to stimulate T cells, we sought to understand the spatial organization of these cells within tumors and their interaction dynamics with T cells both in vivo and in vitro. To differentiate these populations in living spontaneous tumors in vivo, the *PyMTchOVA* allele was crossed on to *Cx3cr1-eGFP* and *Cd11c-mCherry* alleles, generating three uniquely fluorescent populations in the myeloid compartment (Figure 7A). Both DC1 and DC2 subsets were marked red (mCherry only), while TAM1 and TAM2 populations were green (eGFP only) and yellow (mCherry and eGFP), respectively. Using this model, with two-photon intravital imaging, we observed that TAM1 and TAM2 populations are preferentially marginating tightly on tumoral lesions. This zone is one where we had previously found T cells to be preferentially captured (Engelhardt et al., 2012). In contrast, DC subsets typically were

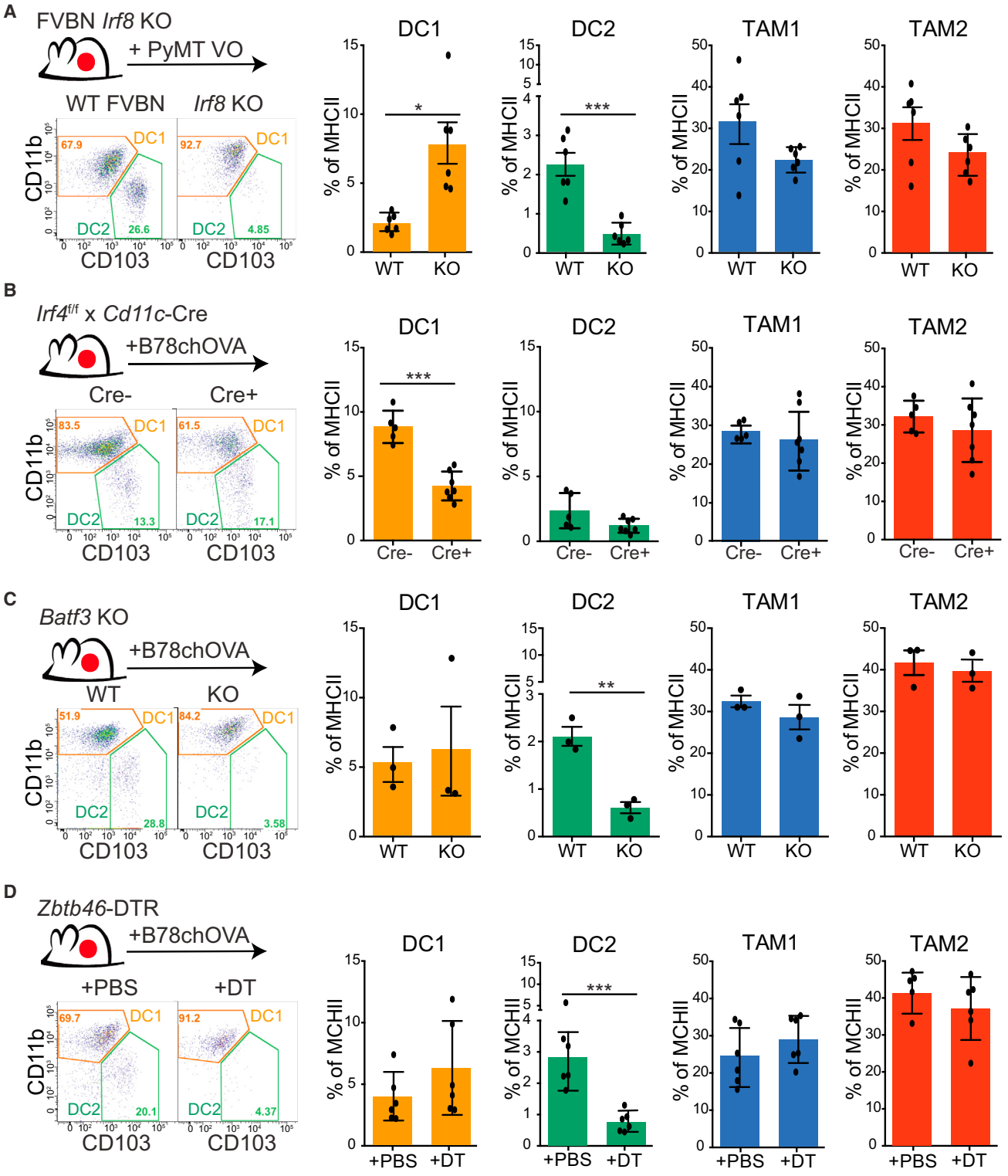

Figure 3. Differential IRF4, IRF8, and Batf3 Requirements for Tumor-Infiltrating APC Populations

(A) Ectopic PyMT-VO tumors from an *Irf8*$^{-/-}$ (KO) compared with control (wild-type [WT]). Relative cell proportions are shown as a percentage of total MHCII^{+} cells. Data are pooled from individual mice (n = 6) from two independent experiments.

(B) Ectopic B78chOVA tumors in *Irf4*$^{f/f}$ x *Cd11c*-Cre^{+} host compared with Cre-negative littermates. Relative cell proportions are shown as a percentage of total MHCII^{+} cells. Data are pooled from individual mice (n = 7) from two independent experiments.

(legend continued on next page)

found in separate collagen-rich zones distal to the tumor lesions, making up nearly 70% of all distally localized APC (Figure 7B).

Since this approach did not fully differentiate between CD11b$^+$ DC1 and CD103$^+$ DC2 cells among those on the margins of tumor foci, we sought to determine whether the few red DCs might preferentially represent exclusively one or the other subset. To delineate the subsets in situ, we utilized live tumor slice imaging, with anti-CD11b antibody staining. Using this, we could distinguish CD11b$^+$ DC1 from CD103$^+$ DC2 subsets in situ in the presence of the red/green fluorescent reporters and found that both CD11b$^+$ and CD11b$^-$ DCs were present at these locations (Figure 7C; Movie S1). We conclude that while TAMs generally represent the dominant cell type at the tumor margin pro-CTL stimulatory APCs nevertheless can be found there, albeit in very low numbers.

Our previous data demonstrated that incoming CTLs engaged in arrest behavior at the tumor margin, and we sought to determine whether these might be taking place with DCs or TAMs or both. In vivo T cell dynamics were analyzed in the red/green reporter system by adoptive transfer of CFP expressing OT-I CD8$^+$ T cells into spontaneous breast tumor-bearing mice, for either intravital or live slice imaging. We observed stable T cell interactions largely confined to the tumor margins, as previously described (Boissonnas et al., 2013; Engelhardt et al., 2012) (Figures 7D and 7E; Movie S2). Although TAM1 interactions dominated all interactions scored, DCs and TAM2s were also well represented in T cell arrests. This demonstrates that DC1/DC2 in the tumor-proximal regions are not incapable nor physically excluded from engaging T cells within tumors but did raise a fundamental question of whether either is intrinsically more capable of engaging T cells.

To answer this, we divorced APC selection from the physical constraints of the tissue and digested tumor to make single-cell suspension and introduced in vitro activated OT-I CTLs and allowed them to form antigen-specific couples. We then quantified the percentage of each APC population that was occupied with a T cell by flow cytometry. This revealed that OT-I T cells couple preferentially with CD103$^+$ DC2 and TAM1/TAM2 subsets (Figure 7F, left panel). However, due to the high frequency of TAM1/TAM2, most T cell-APC couples are formed with TAM1/TAM2 cells (Figure 7F, right panel). We conclude that DC2s contribute to T cell interactions in tumors and when present near the margin are capable of competing for T cell occupancy.

Rare Tumor CD103$^+$ DC2s Are Required for Efficient Adoptive T Cell Therapy

We were surprised to find that the proportions of CD11b$^+$ DC1 and CD103$^+$ DC2 were nearly inverted in a spontaneously regressing EG7 tumor model, hereto after referred to as EG7.2, as compared with a fully aggressive and outgrowing line EG7.1. While the aggressively growing tumors maintained the relative proportions of DCs we observed in all other aggressive tumors (Figure S6A), the spontaneously regressing model contained unusually high numbers of the CD103$^+$ DC2 (Figure S6B). We also observed increased tumor growth in the *Irf8* KO tumor model, which lack CD103$^+$ DC2, but not in *the Irf4* conditional KO model (Figures S6C and S6D). These together suggest that DC2 tumoral abundance may play an important role in tumor control; however, the differences in outgrowth may be caused by many variances in these tumors beyond their populations of myeloid cells and their ability to stimulate CTLs. To formally test whether the CD103$^+$ DC2s are necessary for efficient CTL-mediated tumor regression, we turned to the outgrowing EG7.1 tumor model and performed adoptive T cell therapy of activated tumor specific T cells (Helmich and Dutton, 2001). We performed these experiments in *zDC*-DTR mice, which permitted us to specifically ablate CD103$^+$ DC2 in the tumor (Figure 3D). In order to isolate the effect of the CD103$^+$ DC2 to the site of the tumor and eliminate any effect of LN priming, we designed the experiment to include two strategies: (1) use of activated OT-I CD8$^+$ CTL blasts, which do not require priming in the LN and typically do not traffic there and (2) treatment of animals with the SIP_1R antagonist FTY-720, which prevents LN exit of rare transferred CTL T cells that traffic to the LN. The effect of FTY-720 alone had minimal effects on transferred CTLs to mediate tumor regression (Figure S6E). However, we found that ablation of CD103$^+$ DC2s in the context of FTY-720 had a significant effect on the ability of CTLs to mediated efficient tumor regression, massively slowing T-cell-mediation tumor regression (Figure 8A).

Signatures of Intratumoral CD103$^+$ DC2 Abundance Predict Outcome across Human Cancer

To determine whether a critical role for CD103$^+$ DC2 abundance translated to human tumors, we took advantage of TCGA data (Weinstein et al., 2013; Hoadley et al., 2014) that quantifies relative gene expression from numerous human cancer types with matched outcome data. We used our RNAseq data to select for high level transcripts that characterized CD103$^+$ DC2 and also selected a subset of genes that characterized TAM1/TAM2/CD11b$^+$DC1 cells but were deficient in CD103$^+$ DC2. We identified human homologs of those mouse genes and assayed expression of these genes in TCGA data from all cancer types to assess prognostic associations. In a proportional hazards survival analysis, adjusting the model for cancer type as a covariate, we observed that the individual genes from these populations had only modest prognostic benefits (expressed as hazard ratio [HR]). In order to represent the relative proportion of the two cell types, we defined a ratio of the CD103$^+$ and CD103$^-$ gene expression data and used this as a continuous variable within the Cox analysis. High expression of this ratio was significantly associated with increased overall survival (Benjamini-Hochberg [BH] p = 0.00019) (Figure 8B).

(C) Ectopic B78chOVA tumors in *Batf3* KO compared with WT. Relative cell proportions are graphed as a percentage of total MHCII$^+$. Data are pooled from individual mice (n = 6).

(D) Ectopic B78chOVA tumors in *Zbtb46*-DTR mice receiving acute 24 hr depletion with DT or PBS. Relative cell proportions are graphed as a percentage of total MHCII$^+$ cells. Data are pooled from individual mice (n = 6) from two independent experiments.

All data are representative flow cytometric analysis of CD11b$^+$DC1 and CD103$^+$DC2 populations (gated on CD45$^+$, Ly6C$^-$, MHCII$^+$, and CD24$^+$). Data are shown as mean ± SEM. Statistical significance is indicated by *p < 0.05, **p < 0.01, ***p < 0.001; ns, not statistically significant.

Please cite this article in press as: Broz et al., Dissecting the Tumor Myeloid Compartment Reveals Rare Activating Antigen-Presenting Cells Critical for T Cell Immunity, Cancer Cell (2014), http://dx.doi.org/10.1016/j.ccell.2014.09.007

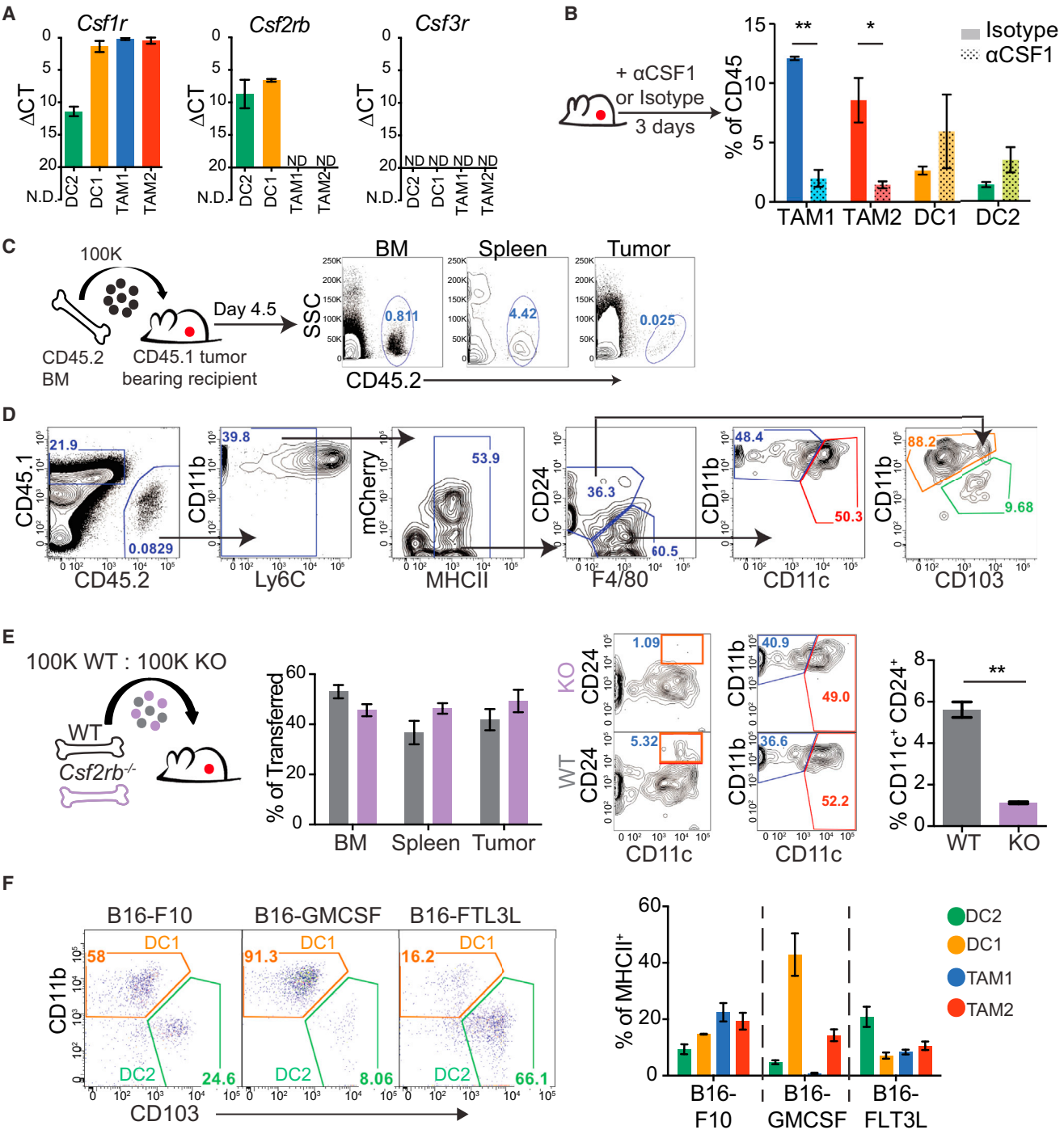

Figure 4. Differential Reliance on M-CSF and GM-CSF Cytokines by Tumor-Infiltrating APC Populations

(A) qPCR of *Csf1r*, *Csf2rb*, and *Csf3r* expression from sorted APCs. Data are presented as mean Δ Ct ± SEM calculated from biological triplicates (n = 3) of individual B78chOVA tumors (N.D., not detected).

(B) Cytometry of tumor APCs after 3 days of αCSF1 (αCSF1, dotted) compared with isotype (filled)-treated tumor animals. Quantified as a percentage of total tumor CD45$^+$ cells, pooled from individual mice (n = 6) from two independent experiments shown as mean ± SEM. Statistical significance is indicated by *p < 0.05, **p < 0.01, ***p < 0.001 (ns, not statistically significant).

(C) Schematic of BM progenitor adoptive transfer and contributions to BM, spleen, and tumor.

(D) Representative cytometry of tumor-arriving congenic cells; gated on CD45.2 and following the gating strategy of Figure 1A.

(E) Competitive BM adoptive transfer of WT versus *Csf2rb* KO GMP progenitors into B78chOVA tumor recipients. Repopulation efficiency is plotted as the percentage of total transferred cells. This is representative gating of tumor arriving GMP cells, WT (gray), KO (purple). Quantification of tumor-arriving DCs is defined by CD24$^+$ CD11c$^+$. Data are pooled from two independent experiments and plotted as mean ± SEM from individual tumors (n = 6).

(legend continued on next page)

This analysis shows that the cell type we identified, when ratioed with its functional opposite, generates a very strong prognostic value for outcome across human cancers. Comparing this "signature" with other previously described "immune scores" shows that the ratio of CD103$^+$/CD103$^-$ genes provides the strongest proimmune survival signal compared with other current analyses of TCGA data, including those based on total T cell abundance (Palmer et al., 2006) and that made by bulk ratio of CD8 T cells to macrophages (CD8/CD68; DeNardo et al., 2011) (Figure 8C). Our score also compares favorably, though opposite in prognosis, for those immune scores associated with poor outcome. It is also notable that CSF1 expression in tumors in these patients also anticorrelates with the CD103/BDCA3 gene ratio measure, although it likewise anticorrelates with total tumor FTL3L levels (Figures S6F and S6G).

Finally, we sought to analyze the TCGA data within individual cancer types. Adjusting for cancer type, a Kaplan-Meier (K-M) plot for all 12 cancers in this data set shows the overall benefit in tumors with a high CD103$^+$/CD103$^-$ gene-expression profile (Figure 8D; unadjusted plot in Figure S6H). The extent of this association is particularly profound in breast cancer, head-neck squamous cell carcinoma, and lung adenocarcinoma (Figures 8E–8G). Overall, this represents an unexpectedly strong immune signature, the more so as it was derived entirely from empirical immunoprofiling in mouse tumor models.

DISCUSSION

A critically important feature of this work is that within the diverse array of myeloid cells at the tumor, a rare population of proimmune DCs exists even in immunoevasive tumors. This contrasts with previous characterizations of the myeloid lineage in tumors that have highlighted their immunosuppressive functions. This study puts a face and a name on a specific subset of intratumoral DCs whose functions one would wish to enhance as part of immunotherapy and serves to begin to demystify the complexity of this critical compartment.

This work provides an understanding of the tumoral myeloid environment as having lineage parallels to other nontransformed tissues. Significant confusion in the current literature of myeloid subpopulations results from inappropriate grouping of cells (e.g., CD11b$^+$) or from lack of a common method for distinguishing the various subpopulations (e.g., CD11c expression). Recent additions to the repertoire of antibody markers and total expression-array analyses of DCs versus macrophages versus monocytes provided significant clarity to this situation (Gautier et al., 2012; Miller et al., 2012). In particular, while conventional DCs are seen to express one or more of markers such as CD24, TAMs are better described through surface expression of F4/80, CD64, and MerTK. To that end, CD11b$^+$ DC1s in tumors appear, by RNA expression and surface expression, to be more closely allied to macrophages. This proximity of these cells has been observed in other peripheral sites (Gautier et al., 2012). In general, a remarkable similarity in IRF4-, IRF8-, and Batf3-dependent origins and surface phenotypes suggests that the overall origins and distinctions of tumor-infiltrating myeloid cells is quite similar to counterparts in normal tissues.

Our studies confirm earlier work showing that mice deficient of *Batf3* failed to spontaneously clear highly immunogenic tumors (Hildner et al., 2008). However, our studies provide the additional insight that the key populations defined by Batf3 and IRF8, but not IRF4 expression, are not only present and functional within tumors but in fact are required for productive responses to adoptively transferred CTLs generated in vitro, after T cells are already primed and in the absence of profound LN involvement. This places at least some of the key Batf3- and now IRF8-dependent cells as playing key roles in repriming within the tumor. Thus, our understanding shifts emphasis from the LN to the tumor for T cell control. Our work also puts these cells in context in the tumor and shows that, while they may be sporadically present on the tumor margins where T cells will encounter their APCs, they are very sparse there. Clinically, this suggests that enhancement of the intratumoral load of these cells will be an important cofactor defining the success of adoptive T cell therapies and broadly that providing restimulation within the tumor represents an important requirement for T cell function at that site. That the requirement for CD103 cells is intratumoral is further supported by our TCGA analysis in which gene-expression data used to assess prognostic value derive exclusively from mRNA taken from the tumor but not the LN.

While our data did not show an absolute dependence on CD103$^+$ DC2 to facilitate adoptive CTL control of tumor outgrowth, the effect was profound. It is not clear whether residual T-cell-dependent control in the DT-treated cohort might represent myeloid-independent activity of these cells, a compensatory role by other myeloid cells (e.g., CD11b$^+$ DC1, which stimulate CTL extremely weakly in vitro) or merely our inability to fully eliminate the CD103$^+$ DC2 population. To that last possibility, it will be increasingly important to more effectively manipulate the relative population densities of myeloid cells, sparing the CD103$^+$ DC2 or even providing means to enhance them. Our demonstration of enhanced CD103$^+$ DC2 generation in FTL3L expressing tumors provides a compelling rationale as to why such therapy may work and indeed may be synergistic with T cell therapies such as anti-CTLA4 (Curran and Allison, 2009). Conversely, the efficacy of α-CSF1 therapies (Ries et al., 2014; Strachan et al., 2013) may be in part due to the sparing of CD103$^+$ DC2 under such blockade, as demonstrated in our work.

Despite significantly increased clarity of the identities of intratumoral myeloid populations and their similarities to those in normal tissues, much remains to be elucidated concerning the additional functional diversity of the intratumoral APCs. In particular, the role of CD11b$^+$ DC1 in the tumor remains obscure. Their transcriptional profiling and surface markers may place them closer in identity to TAMs as compared with CD103$^+$ DC2, which is found in other macrophage populations from healthy peripheral sites (Gautier et al., 2012). We also note that these highly

(F) Cytometry of CD11b$^+$ DC1 and CD103$^+$ DC2 populations (gated on CD45$^+$, Ly6C$^-$ MHCII$^+$, CD24$^+$) between ectopic B16-F10, B16-GMCSF, and B16-FLT3L cytokine-expressing tumors. Populations are presented as the percentage of total MHCII$^+$ cells for each tumor. Data are pooled from three independent experiments, plotted as mean ± SEM from individual tumors (n = 6).
See also Figure S3.

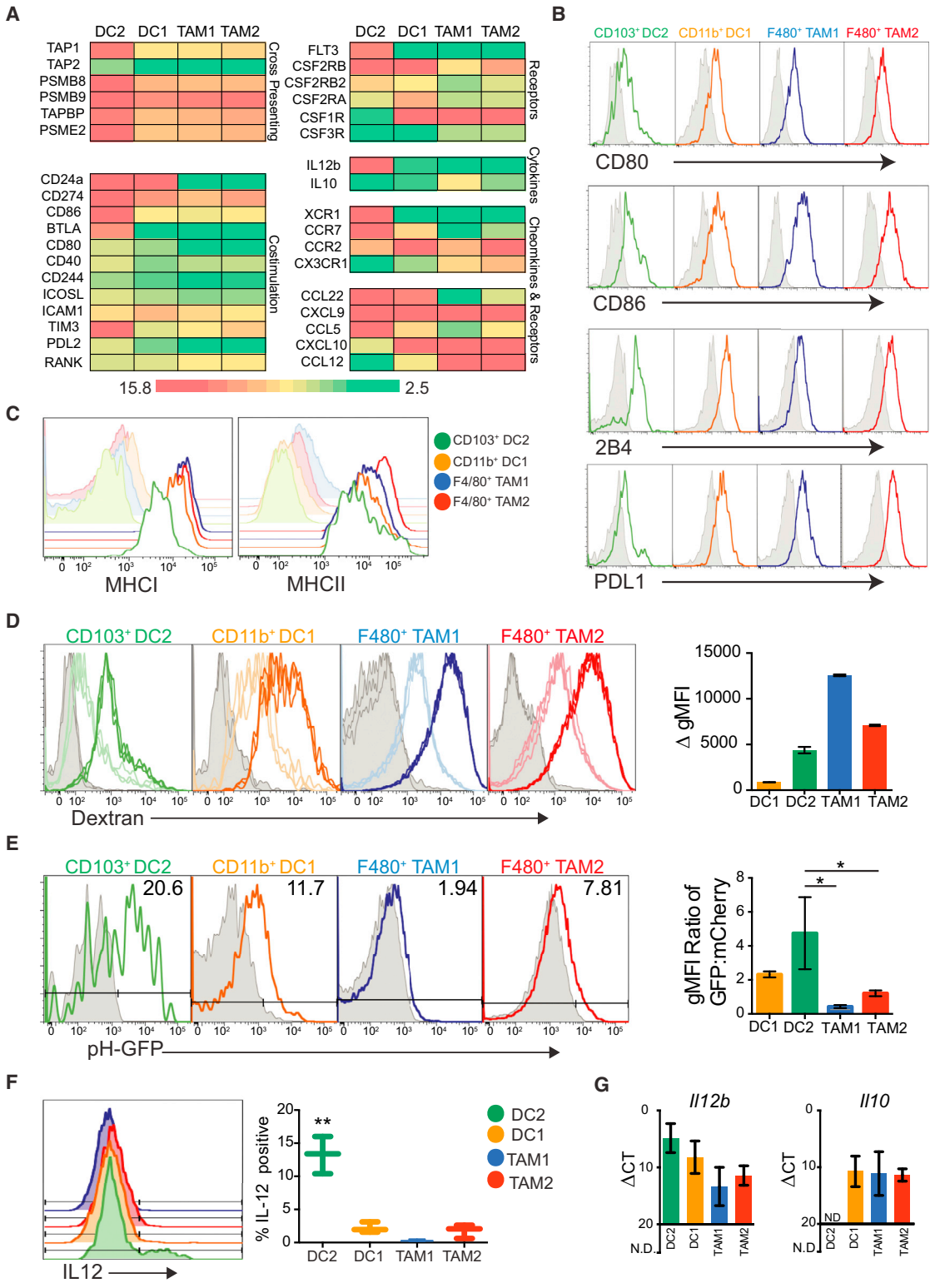

Figure 5. Unique Antigen Processing and Presentation Capabilities of CD103+ DC2

(A) Heat map of log_2-transformed expression from RNAseq across populations for selected genes involved in cross-presenting, cytokine and chemokine production, and costimulation. The color scale is defined as green = bottom 20th percentile and red = top 80th percentile, with 20th to 80th percentile graduated and centered at yellow (50th percentile). Data are from biological triplicates of sorted cells.

(B) Cytometry of surface protein levels of ligands for T-cell-regulatory molecules (colored) as compared with respective isotypes (gray).

(C) Cytometry of MCHI and MHCII (colored) expression compared with respective isotype (shaded).

(legend continued on next page)

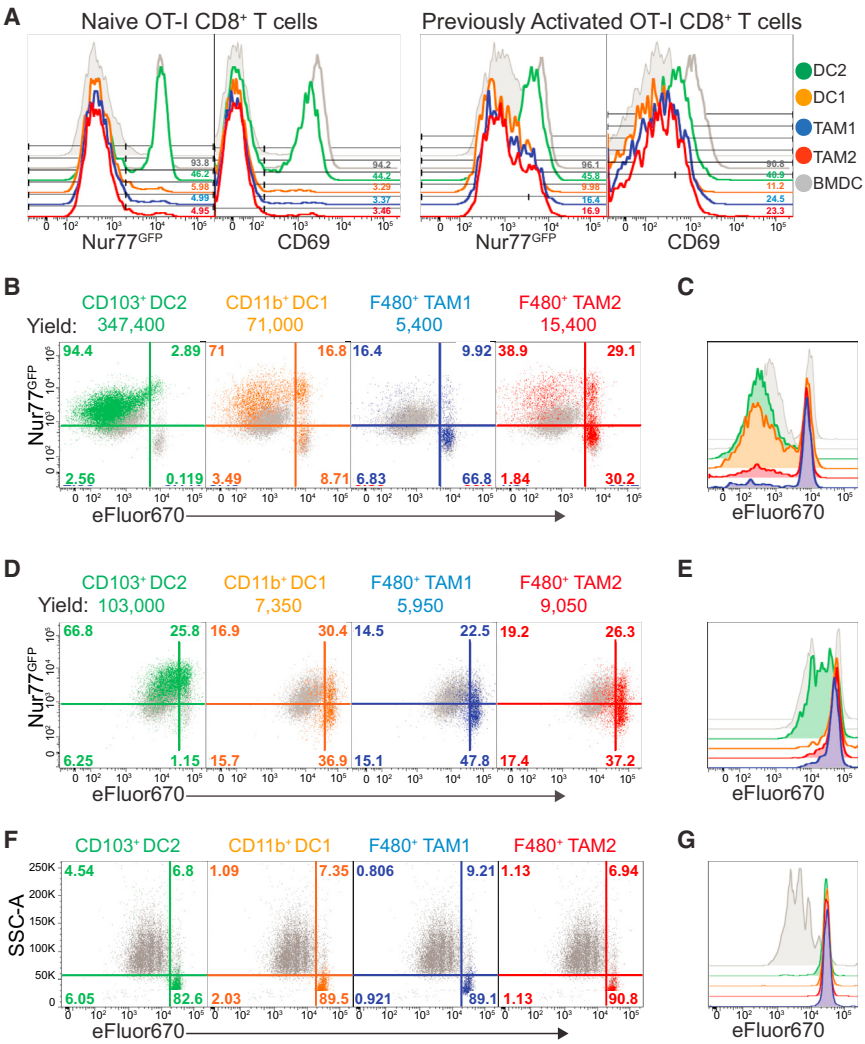

Figure 6. CD103$^+$ DCs Are Superior T Cell Stimulators for Naive and Activated CD8$^+$ T cells

(A) Flow cytometry of early activation markers Nur77^{GFP} and CD69 (12 hr) on naive or previously activated OT-I CD8$^+$ T cells cultured on sorted APC populations directly from tumors.

(B) Representative cytometry of naive OT-I CD8$^+$ T cell proliferation, measured by dye dilution of eFluor670 plotted against Nur77^{GFP} (as measure of TCR triggering), at 72 hr following coculture with tumor APC populations. The total cell yield counts are listed above the graphs.

(C) Histogram overlay of naive T cell proliferation between tumor APCs.

(D) Representative cytometry of T cell proliferation, measured by dye dilution of eFluor670 plotted against Nur77^{GFP} at 72 hr for previously activated OT-I CD8$^+$ T cell blasts cultured on tumor APC populations. Total cell yield counts are listed above the graphs.

(E) Histogram overlay of previously activated OT-I CD8$^+$ T cell proliferation across tumor APCs.

(F) Representative cytometry of T cell proliferation, measured by dye dilution of eFluor670, at 72 hr for naive OT-II CD4$^+$ T cells cultured on tumor APC populations. Representative flow plots are from two independent experiments.

(G) Histogram overlay of naive OT-II CD4$^+$ T cell proliferation across tumor APCs.

All data are from the ectopic B78chOVA tumor model: T cells + BMDC (shaded gray), T cells + BMDC + SL8 (unshaded gray), T cells + tumor APCs (respective colored histograms). These are plated at 20,000 T cells: 4,000 APC. Representative flow plots are from four independent experiments, unless noted. See also Figure S5.

resemble recently described "DC-T_h2," defined by their reliance on the transcription factor IRF4, expression of CD301b and PDL2, and ability to effectively prime Th2 responses (Gao et al., 2013; Kumamoto et al., 2013; Williams et al., 2013). At present, we failed to find a DC population that could robustly stimulate CD4 T cells when taken directly from the tumor; however, DC1 and DC2 could be rescued upon add back of peptide, suggesting either that the MHCII processing pathway is not highly active in these cells or that our digest conditions affect MHCII antigen loading. Regardless, this may reinforce the hypothesis that the absence of effective T cell help and its attendant γc cytokine production are critical missing links in the tumor microenvironment.

Our study of these cell types now brings to the forefront many spatiotemporal issues about how the various myeloid populations interface with tumors, with one another, and with T cells. While it is clear from our imaging that the marginating cells are dominated by TAM1 and TAM2, the nature of "APC selection" by T cells is not fully resolved. Do CTLs with particular activation choose particular subsets of myeloid cells, and conversely, does

(D) Cytometry of ex vivo dextran uptake across populations. The gray shows no dextran. The light histogram shows dextran binding at 4°C, and dark histogram shows dextran uptake at 37°C, displayed in triplicate. Delta geometric mean fluorescence intensity (gMFI) for each population is plotted as mean ± SEM. Data are representative of two independent experiments (n = 6).

(E) Cytometry analysis of relative pH of endocytic compartments across populations. B78 tumor cells were transfected with the ratiometric pH construct, N1-mCherry-pHlourin. Representative histograms show florescence of pHluorin in mCherry$^+$ cells, where less pH-GFP represents a more acidic environment. Gray histograms are respective populations from a non-pHluorin expressing control tumor (B78 parental). Data are summarized as the ratio of gMFI between GFP and mCherry fluorescence. Data are presented as mean ratio ± SEM, pooled from three independent experiments.

(F) Intracellular cytokine stain of IL-12 in populations. The percentage of IL-12$^+$ cells is quantified across each population. Data are pooled from two independent experiments (n = 3) and plotted as mean ± SEM. Statistical significance is indicated by *$p < 0.05$.

(G) *Il12b* and *Il10* transcript levels, measured by qPCR. Data are presented as mean Δ Ct ± SEM calculated from biological triplicates (n = 3) of individual tumors (N.D., not detected).

All data are from the ectopic B78chOVA tumor model. See also Figure S4.

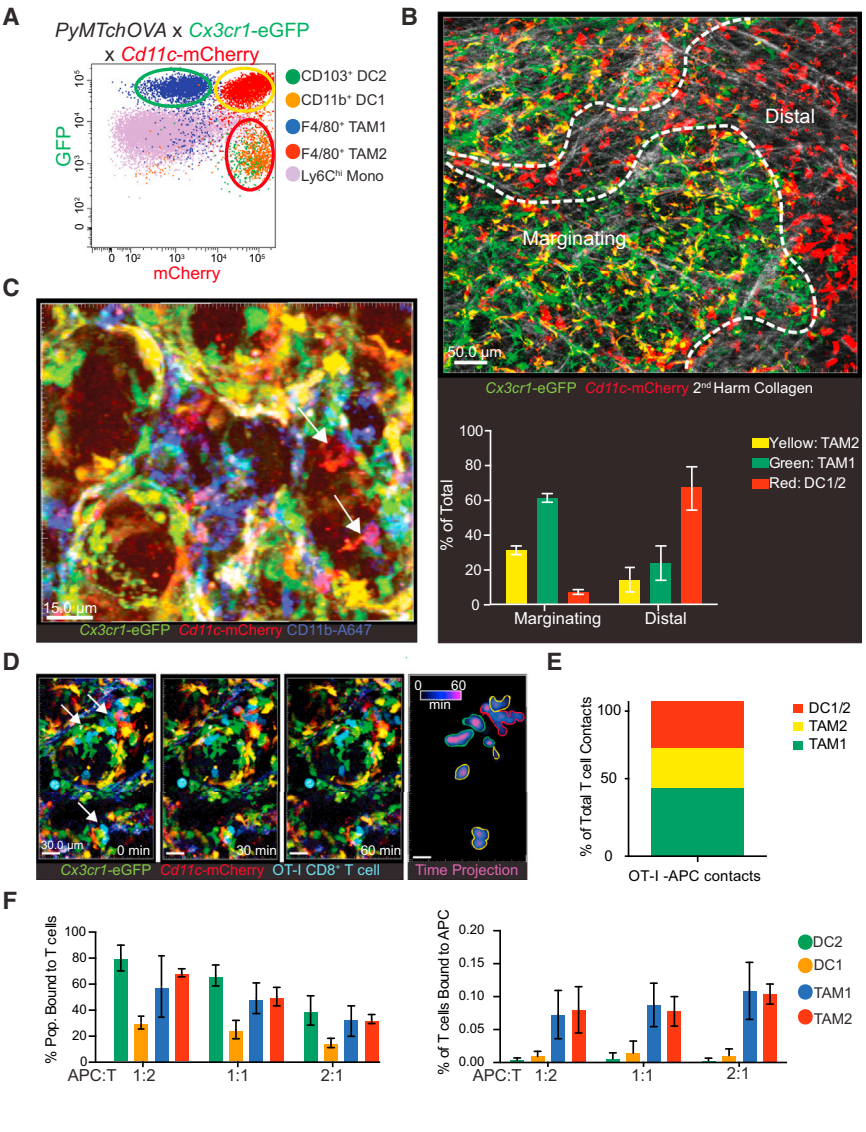

Figure 7. Intravital and Slice Imaging Reveals that CD11b+ DC1 and CD103+ DC2 Are Sparse Near Tumor Margins yet Can Interact with T Cells When Present There

(A) Representative cytometry of tumor APCs in *PyMTchOVA* x *Cx3cr1*-eGFP × *Cd11c*-mCherry. Populations as previously defined are plotted as mCherry versus GFP. Green, yellow, and red circles indicate the fluorescent profile that each population displays in this model. Red (mCherry only cells), yellow (mCherry and GFP double-positive cells), and green (GFP only cells) are shown. By flow cytometry, DC1/DC2 populations fall in the Cherry-only population, while TAM1 and TAM2 comprise the yellow and green populations, respectively.

(B) Intravital 2-photon representative still image of an early carcinoma lesion from a *PyMTchOVA* × *Cx3cr1*-eGFP × *Cd11c*-mCherry reporter. Regions indicated with a dashed line, marked either distal or marginating to lesions, were determined with a combination of mCherry fluorescence and collagen structure. Collagen fibers are marked (white) by second harmonic generation. The scale bar represents 50 μm. (Inset) Quantification of the proximal/distal location of the APCs within the tumor. Data pooled from four independent imaging runs, presented as mean ± SEM.

(C) Representative confocal still image from live tumor slices in *PyMTchOVA* × *Cx3cr1*-eGFP × *Cd11c*-mCherry tumors, stained with CD11b-A647 antibody. mCherry only cell (arrowhead DC2, red) and mCherry+ CD11b+ cell (arrow DC1, purple) in the tumor. Scale bar 15 μm.

(D) Representative image sequence of CFP expressing OT-1 CD8+ T cells (blue) dynamically interacting with APC cells in the *PyMTchOVA* × *Cx3cr1*-eGFP × *Cd11c*-mCherry model by live slice confocal imaging 4 days after T cell transfer at 0, 30, and 60 min. The arrows indicate T cell interactions with red (DC1/DC2), green (TAM1), or yellow (TAM2) cells. The scale bar represents 30 μm. The last panel displays time projection of CFP expressing T cells through 60 min imaging timeframe, with outline color dictated by APC of contact.

(E) APC-T cell contacts in vivo as a percentage of the total T cell couples observed. Accumulated data are shown of four different positions imaged for 30 min in two independent intravital 2 photon imaging runs. Contacts were scored manually by counting physical contact made between T cells and red, yellow, and green APCs. The color of bar represents the APC of contact (red: CD103+, CD11b+ DC1; green: TAM1; yellow: TAM2).

(F) Ex vivo T-cell-coupling assay with digested tumor positively selected for CD45+ cells with previously activated OT-I CD8+ T cell. Data are calculated as percentage of T cells couples within each of the populations (left) and as a total percentage of T cell couples (right). Data are pooled from two independent experiments, plotted as mean ± SEM.

See also Movies S1 and S2.

the in situ interaction of T cells with CD103+ DC2 give them abilities to kill so long as they do not encounter a TAM in the interim? Many of these types of questions will require elaboration of spectral labeling methods. In addition, these types of approaches will require significant adoption and/or development of biosensor-like reporters to determine where and when complete TCR signaling is taking place.

Finally, a very important finding of this study relates to the applicability of the myeloid delineation to multiple human tumors. Using bioinformatics based on these populations, we observed that CD103+ DC2-enriched transcripts, taken from mouse models and expressed as a ratio with an equivalent selection from the TAM/DC1 populations, provides a strong prognostic signal in TCGA data, across multiple tumor types. The fact that this "signature" correlates with patient survival better than other published signatures provides an additional and compelling reason to suggest that this population is critical for robust tumor control in mice and humans. Clearly, additional profiling of these populations in context of immunotherapies will be required to test this further and should be undertaken alongside all further immunotherapy trials. It will be particularly interesting to determine whether patients having CD103/BDCA3 "high" tumors will represent better responders to checkpoint blockade. In sum, it is clear that these rare cells should now be a target to augment their numbers as well as a biomarker that may define those whose immune response is well positioned to eliminate cancers.

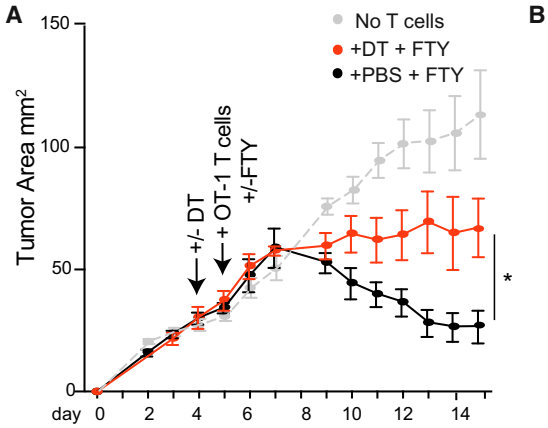

B

Gene/Signat.	Type	HR [95% CI]	p value	BH p val
CD103+/- RATIO	**RATIO**	**0.792 [0.719-0.872]**	**2.23E-06**	**6.47E-05**
KIT	CD103+	0.896 [0.826-0.972]	0.00841	**0.0264**
CCR7	CD103+	0.905 [0.84-0.976]	0.00912	**0.0264**
CD103+ Genes	CD103+	0.907 [0.838-0.981]	0.0152	**0.0399**
BATF3	CD103+	1.1 [1.02-1.2]	0.0165	**0.0399**
FTL3	CD103+	0.862 [0.745-0.997]	0.0458	0.0781
ZBTB46	CD103+	1.07 [0.985-1.16]	0.11	0.168
IRF8	CD103+	0.952 [0.886-1.02]	0.182	0.254
BTLA	CD103+	0.957 [0.879-1.04]	0.306	0.403
MYCL1	CD103+	0.969 [0.892-1.05]	0.459	0.532
CLEC9A	CD103+	0.976 [0.895-1.06]	0.583	0.604
C5AR1	CD103-	1.12 [1.06-1.19]	0.00014	**0.00203**
LYVE1	CD103-	1.15 [1.06-1.24]	0.00062	**0.00502**
ABCC3	CD103-	1.17 [1.07-1.29]	0.000693	**0.00502**
MRC1	CD103-	1.14 [1.05-1.23]	0.00162	**0.0094**
SIGLEC1	CD103-	1.11 [1.04-1.19]	0.00202	**0.00976**
CD103- Genes	CD103-	1.12 [1.03-1.21]	0.00541	**0.02**
STAB1	CD103-	1.09 [1.03-1.16]	0.00551	**0.02**
C1QB	CD103-	1.1 [1.01-1.19]	0.0218	0.052
C1QA	CD103-	1.1 [1.01-1.19]	0.0233	0.052
TMEM37	CD103-	0.889 [0.801-0.987]	0.0278	0.0576
MERTK	CD103-	0.93 [0.869-0.996]	0.0392	0.0758
C1QC	CD103-	1.07 [0.986-1.16]	0.106	0.168
TMEM119	CD103-	1.05 [0.976-1.13]	0.184	0.254
MS4A7	CD103-	1.04 [0.961-1.13]	0.322	0.406
APOE	CD103-	1.04 [0.943-1.14]	0.438	0.529
CYP4F18	CD103-	1.03 [0.951-1.11]	0.477	0.532
TREM2	CD103-	1.02 [0.943-1.11]	0.583	0.604
TLR7	CD103-	1.01 [0.937-1.08]	0.868	0.868

C

Signature	OS Assoc.	HR [95% CI]	p value	BH p val
CD103+/- Ratio	**Increased**	**0.79 [0.719-0.87]**	**2.23E-06**	**1.34E-05**
T Cell	Increased	0.848 [0.76-0.93]	0.00096	0.00144
CD8/CD68 Ratio	Increased	0.908 [0.85-0.96]	0.00315	0.00378
Proliferation	Decreased	1.19 [1.08-1.31]	0.00047	0.00142
CSR/Wound	Decreased	1.18 [1.07-1.3]	0.00092	0.00144
IFNG	Decreased	1.12 [1.03-1.21]	0.00479	0.00479

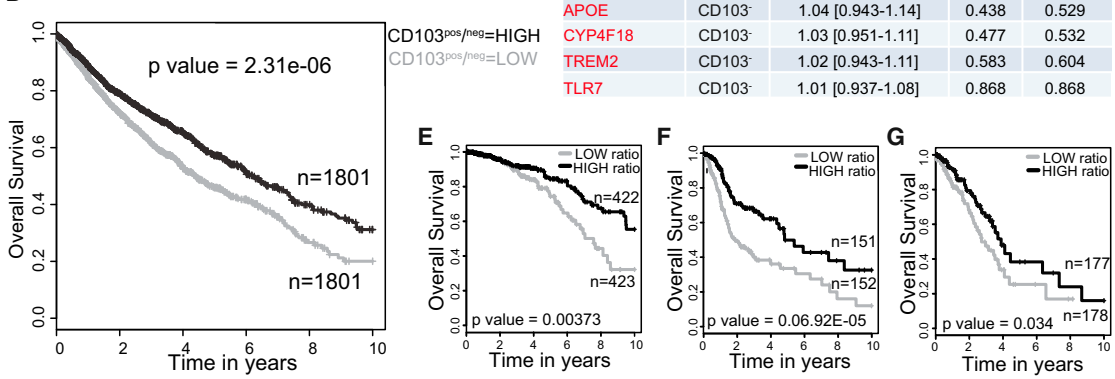

Figure 8. Rare CD103+ DC2 Population at the Tumor Is Required for Efficient Adoptive CTL Therapy

(A) Tumor growth curve plotted as tumor area (mm^2) over time for EG7.1 in *zDC*-DTR hosts. The arrows indicate time of intraperitoneal DT/PBS administration, and intravenous transfer of 5×10^6 previously activated OT-I $CD8^+$ T cells. DT/PBS was subsequently administered every third day, and FTY-720/saline was subsequently administered every other day throughout time course. Representative data are presented as mean tumor area ± SEM (n = 4) from two independent experiments. Statistical significance is indicated by *p < 0.05.

(B) Comparison of prognostic value of $CD103^+/CD103^-$ ratio gene signal as compared with the individual genes (either $CD103^+$ specific, green, or TAM1/TAM2/CD11b DC1 specific genes, red) using TCGA data sets in a multivariate COX proportional hazards survival analysis adjusting for cancer type as a covariate. Data are expressed as HR with 95% confidence intervals, where a value <1 means increased overall survival (OS); >1 means decreased OS for genes with BH p values < 0.05 (bolded values).

(C) Comparison of the prognostic value of the $CD103^+/CD1033^-$ ratio gene signal with several published prognostic gene signatures using TCGA data sets in a multivariate COX proportional hazards survival analysis adjusting for cancer type as a covariate. Data are expressed as HR with 95% confidence intervals, where a value <1 means increased overall survival (OS); >1 means decreased OS for genes with BH p values < 0.05.

(D) K-M plot across all 12 cancer types in human TCGA data sets, adjusting for cancer type based on high $CD103^+/CD1033^-$ gene ratio and low $CD103^+/CD1033^-$ ratio expressers (median split/cancer).

(E) K-M plot for overall survival of breast cancer patients in TCGA data set. Data are parsed on high $CD103^+/CD1033^-$ gene ratio and low $CD103^+/CD1033^-$ ratio expressers.

(F) K-M plot for overall survival of head and neck squamous cell carcinoma patients in TCGA data set. Data are parsed on high $CD103^+/CD1033^-$ gene ratio and low $CD103^+/CD1033^-$ ratio expressers.

(G) K-M plot for overall survival of lung adenocarcinoma patients in TCGA data set. Data are parsed on high $CD103^+/CD1033^-$ gene ratio and low $CD103^+/CD1033^-$ ratio expressers.

See also Figure S6.

EXPERIMENTAL PROCEDURES

Mouse Tumors

PyMT-ChOVA transgenic C57BL/6 founder mice were as described (Engelhardt et al., 2012), and offspring were screened for the *PyMT-ChOVA* transgene by PCR and monitored for tumors and used at 20 to 30 weeks of age. B78ChOVA is a variant of B78 (Graf et al., 1984) and is generated and used as described in Supplemental Experimental Procedures. All additional strain information can be found in supplemental methods. All mice were maintained under specific pathogen free (SPF) conditions and treated in accordance with the regulatory standards of the NIH and American Association of Laboratory Animal Care standards and are consistent with the UCSF Institution of Animal Care and Use Committee (IACUC approval: AN106779-01A).

Flow Cytometry

All antibodies were purchased from BD Pharmingen, eBioscience, Invitrogen, Biolegend, and the UCSF hybridoma core or were produced in the Krummel Lab. For surface staining, cells were incubated with anti-Fc receptor antibody (clone 2.4G2) and stained with antibodies in PBS + 2% fetal calf serum for 30 min on ice. Viability was assessed by staining with fixable Live/Dead Zombie (Biolegend) or 4′,6-diamidino-2-phenylindole. For intracellular staining, mice were injected with 10 μg/g of body weight with Brefeldin A (Cayman) 6 hr prior to harvest. Cells were stained with antibodies against surface markers and then fixed with 2% paraformaldehyde for 10 min at 25°C and permeabilized with 0.2% saponin then stained with target antibody. All flow cytometry was performed on a BD Fortessa flow cytometer. Analysis of flow cytometry data was done using Flowjo (Treestar). Cell sorting was performed using a BD FACS Aria II.

Human Samples

Tissue was vigorously minced with surgical scissors and transferred to a 25 ml Erlenmeyer with magnetic stir bar with 3 mg/ml collagenase A (Roche) and 50 U/ml DNase I (Roche) per 0.3 g of tissue for 1 hr at 37°C and 5% CO_2 with constant agitation. Samples are then filtered through a 70 μm filter, spun down, and resuspended for staining. For all human samples, informed consent was obtained from all subjects, and work was performed in accordance with institutional review board (IRB) approval (IRB number 13-12246, 12/06/2013-12/05/2014).

TCGA Bioinformatics Analysis

Clinical expression analysis uses genome-wide mRNA levels (Illumina mRNA-seq) from 3,602 patient tumor samples representing 12 cancer types (845 breast, 265 ovarian, 303 head and neck squamous, 122 bladder, 168 glioblastoma, 190 colon, 173 acute myeloid leukemia, 72 rectal, 355 lung adenocarcinoma, 259 lung squamous, 480 kidney, and 370 uterine cancers), normalized, and combined into a single data set by the TCGA PanCancer working group as published (Weinstein et al., 2013; Hoadley et al., 2014) (data are in the TCGA Data Portal [https://tcga-data.nci.nih.gov/tcga/] and available as syn1715755 at https://www.synapse.org/). The CD103$^+$/CD103$^-$ ratio signature is calculated as the log of the mean expression of CD103$^+$ DC genes divided by the mean expression of the CD103$^-$ DC genes, followed by *Z* score standardization (mean = 0, SD = 1; gene list in Figure 8C). We also evaluate published T cell (Palmer et al., 2006), proliferation (Wolf et al., 2014), CSR/wound (Chang et al., 2005), and gamma interferon (Viigimaa et al., 2010) signatures as published, along with a CD8/CD68 expression ratio (DeNardo et al., 2011). Overall survival data were obtained from the TCGA portal (downloaded 6/2013) (Weinstein et al., 2013) and survival analysis performed using Cox proportional hazards modeling in a multivariate model adjusting for cancer type. Log-rank p values are used to assess significance after adjusting for multiple comparisons using the BH method (Bejamini and Hochberg, 1995). K-M survival plots are generated using the Survival package in R. In the all-data KM plot (Figure 8E), we adjusted for cancer type by classifying each sample as "high" or "low" using that cancer types' median value of the CD103$^+$/CD103$^-$ ratio signature.

Statistical Analysis

Statistical analyses were performed using GraphPad Prism software. Unless specifically noted, all data are representative of more than three separate experiments. Error bars represent SEM calculated using Prism and are derived from triplicate experimental conditions. Specific statistical tests used were paired and unpaired t tests, and all p values less than 0.05 were considered statistically significant.

ACCESSION NUMBERS

The NCBI Gene Expression Omnibus (GEO) accession number for the RNASeq data reported in this paper is GSE61462.

SUPPLEMENTAL INFORMATION

Supplemental Information includes Supplemental Experimental Procedures, six figures, and two movies and can be found with this article online at http://dx.doi.org/10.1016/j.ccell.2014.09.007.

AUTHOR CONTRIBUTIONS

M.L.B. designed and performed experiments unless specified. M.B. participated in depletions and cell purifications for RNAseq. B.B. performed imaging experiments and analyses. A.E.N. performed some flow cytometry. J.L.P., D.J.E., and A.B. performed RNAseq and analysis. M.D.R. and A.D. supplied clinical samples. D.L.B. supplied critical reagents. S.A. supplied critical input on analysis of cross-presentation. A.I.S. supplied mice for IRF4 analysis. D.M.W. performed analysis of TCGA data. M.F.K. conceived and participated in design and interpretation of experiments. M.L.B. and M.F.K. wrote, revised, and edited the manuscript, and M.B. and B.B. edited the manuscript.

ACKNOWLEDGMENTS

We thank L.L. Lanier, J. Roose, and L. Fong for advice and C. Guillard and S. Kogan for the generous sharing of materials. This work was supported by NIH grants U01CA105379, U54 CA163123. M.L. Broz was supported by the Genentech Predoctoral Research Fellowship, the Margaret A. Cunningham Immune Mechanisms in Cancer Research Fellowship, and the ARCS Scholarship. We thank K. Corbin for imaging assistance, M.B. Headley for critical reading of the manuscript, and C. Lin for administrative assistance. The signature in Figure 8 is the subject of provisional US Patent Novel Tumor Immune Infiltrate Genetic Signatures.

Received: July 18, 2014
Revised: August 28, 2014
Accepted: September 19, 2014
Published: October 16, 2014

REFERENCES

Bejamini, Y., and Hochberg, Y. (1995). Controlling the false discovery rate: a practical and powerful approach to multiple testing. J. R. Stat. Soc., B *57*, 289–300.

Boissonnas, A., Licata, F., Poupel, L., Jacquelin, S., Fetler, L., Krumeich, S., Théry, C., Amigorena, S., and Combadière, C. (2013). CD8$^+$ tumor-infiltrating T cells are trapped in the tumor-dendritic cell network. Neoplasia *15*, 85–94.

Chang, H.Y., Nuyten, D.S., Sneddon, J.B., Hastie, T., Tibshirani, R., Sørlie, T., Dai, H., He, Y.D., van't Veer, L.J., Bartelink, H., et al. (2005). Robustness, scalability, and integration of a wound-response gene expression signature in predicting breast cancer survival. Proc. Natl. Acad. Sci. USA *102*, 3738–3743.

Cheong, C., Matos, I., Choi, J.H., Dandamudi, D.B., Shrestha, E., Longhi, M.P., Jeffrey, K.L., Anthony, R.M., Kluger, C., Nchinda, G., et al. (2010). Microbial stimulation fully differentiates monocytes to DC-SIGN/CD209(+) dendritic cells for immune T cell areas. Cell *143*, 416–429.

Cortez-Retamozo, V., Etzrodt, M., Newton, A., Rauch, P.J., Chudnovskiy, A., Berger, C., Ryan, R.J., Iwamoto, Y., Marinelli, B., Gorbatov, R., et al. (2012). Origins of tumor-associated macrophages and neutrophils. Proc. Natl. Acad. Sci. USA *109*, 2491–2496.

Curran, M.A., and Allison, J.P. (2009). Tumor vaccines expressing flt3 ligand synergize with ctla-4 blockade to reject preimplanted tumors. Cancer Res. *69*, 7747–7755.

Curran, M.A., Montalvo, W., Yagita, H., and Allison, J.P. (2010). PD-1 and CTLA-4 combination blockade expands infiltrating T cells and reduces regulatory T and myeloid cells within B16 melanoma tumors. Proc. Natl. Acad. Sci. USA *107*, 4275–4280.

DeNardo, D.G., Brennan, D.J., Rexhepaj, E., Ruffell, B., Shiao, S.L., Madden, S.F., Gallagher, W.M., Wadhwani, N., Keil, S.D., Junaid, S.A., et al. (2011). Leukocyte complexity predicts breast cancer survival and functionally regulates response to chemotherapy. Cancer discovery *1*, 54–67.

Dranoff, G. (2002). GM-CSF-based cancer vaccines. Immunol. Rev. *188*, 147–154.

Dzionek, A., Fuchs, A., Schmidt, P., Cremer, S., Zysk, M., Miltenyi, S., Buck, D.W., and Schmitz, J. (2000). BDCA-2, BDCA-3, and BDCA-4: three markers for distinct subsets of dendritic cells in human peripheral blood. J. Immunol. *165*, 6037–6046.

Engelhardt, J.J., Boldajipour, B., Beemiller, P., Pandurangi, P., Sorensen, C., Werb, Z., Egeblad, M., and Krummel, M.F. (2012). Marginating dendritic cells of the tumor microenvironment cross-present tumor antigens and stably engage tumor-specific T cells. Cancer Cell *21*, 402–417.

Gao, Y., Nish, S.A., Jiang, R., Hou, L., Licona-Limón, P., Weinstein, J.S., Zhao, H., and Medzhitov, R. (2013). Control of T helper 2 responses by transcription factor IRF4-dependent dendritic cells. Immunity *39*, 722–732.

Gautier, E.L., Shay, T., Miller, J., Greter, M., Jakubzick, C., Ivanov, S., Helft, J., Chow, A., Elpek, K.G., Gordonov, S., et al.; Immunological Genome Consortium (2012). Gene-expression profiles and transcriptional regulatory pathways that underlie the identity and diversity of mouse tissue macrophages. Nat. Immunol. *13*, 1118–1128.

Geissmann, F., Manz, M.G., Jung, S., Sieweke, M.H., Merad, M., and Ley, K. (2010). Development of monocytes, macrophages, and dendritic cells. Science *327*, 656–661.

Graf, L.H., Jr., Kaplan, P., and Silagi, S. (1984). Efficient DNA-mediated transfer of selectable genes and unselected sequences into differentiated and undifferentiated mouse melanoma clones. Somat. Cell Mol. Genet. *10*, 139–151.

Guermonprez, P., Valladeau, J., Zitvogel, L., Théry, C., and Amigorena, S. (2002). Antigen presentation and T cell stimulation by dendritic cells. Annu. Rev. Immunol. *20*, 621–667.

Hanahan, D., and Weinberg, R.A. (2011). Hallmarks of cancer: the next generation. Cell *144*, 646–674.

Haniffa, M., Shin, A., Bigley, V., McGovern, N., Teo, P., See, P., Wasan, P.S., Wang, X.N., Malinarich, F., Malleret, B., et al. (2012). Human tissues contain CD141hi cross-presenting dendritic cells with functional homology to mouse CD103$^+$ nonlymphoid dendritic cells. Immunity *37*, 60–73.

Hashimoto, D., Miller, J., and Merad, M. (2011). Dendritic cell and macrophage heterogeneity in vivo. Immunity *35*, 323–335.

Helmich, B.K., and Dutton, R.W. (2001). The role of adoptively transferred CD8 T cells and host cells in the control of the growth of the EG7 thymoma: factors that determine the relative effectiveness and homing properties of Tc1 and Tc2 effectors. J. Immunol. *166*, 6500–6508.

Hildner, K., Edelson, B.T., Purtha, W.E., Diamond, M., Matsushita, H., Kohyama, M., Calderon, B., Schraml, B.U., Unanue, E.R., Diamond, M.S., et al. (2008). Batf3 deficiency reveals a critical role for CD8alpha$^+$ dendritic cells in cytotoxic T cell immunity. Science *322*, 1097–1100.

Hoadley, K.A., Yau, C., Wolf, D.M., Cherniack, A.D., Tamborero, D., Ng, S., Leiserson, M.D., Niu, B., McLellan, M.D., Uzunangelov, V., et al.; Cancer Genome Atlas Research Network (2014). Multiplatform analysis of 12 cancer types reveals molecular classification within and across tissues of origin. Cell *158*, 929–944.

Kraman, M., Bambrough, P.J., Arnold, J.N., Roberts, E.W., Magiera, L., Jones, J.O., Gopinathan, A., Tuveson, D.A., and Fearon, D.T. (2010). Suppression of antitumor immunity by stromal cells expressing fibroblast activation protein-alpha. Science *330*, 827–830.

Kumamoto, Y., Linehan, M., Weinstein, J.S., Laidlaw, B.J., Craft, J.E., and Iwasaki, A. (2013). CD301b$^+$ dermal dendritic cells drive T helper 2 cell-mediated immunity. Immunity *39*, 733–743.

Kusmartsev, S., Nagaraj, S., and Gabrilovich, D.I. (2005). Tumor-associated CD8$^+$ T cell tolerance induced by bone marrow-derived immature myeloid cells. J. Immunol. *175*, 4583–4592.

Leach, D.R., Krummel, M.F., and Allison, J.P. (1996). Enhancement of antitumor immunity by CTLA-4 blockade. Science *271*, 1734–1736.

Lewis, C.E., and Pollard, J.W. (2006). Distinct role of macrophages in different tumor microenvironments. Cancer Res. *66*, 605–612.

Meredith, M.M., Liu, K., Darrasse-Jeze, G., Kamphorst, A.O., Schreiber, H.A., Guermonprez, P., Idoyaga, J., Cheong, C., Yao, K.H., Niec, R.E., and Nussenzweig, M.C. (2012). Expression of the zinc finger transcription factor zDC (Zbtb46, Btbd4) defines the classical dendritic cell lineage. J. Exp. Med. *209*, 1153–1165.

Miller, J.C., Brown, B.D., Shay, T., Gautier, E.L., Jojic, V., Cohain, A., Pandey, G., Leboeuf, M., Elpek, K.G., Helft, J., et al.; Immunological Genome Consortium (2012). Deciphering the transcriptional network of the dendritic cell lineage. Nat. Immunol. *13*, 888–899.

Movahedi, K., Laoui, D., Gysemans, C., Baeten, M., Stangé, G., Van den Bossche, J., Mack, M., Pipeleers, D., In't Veld, P., De Baetselier, P., and Van Ginderachter, J.A. (2010). Different tumor microenvironments contain functionally distinct subsets of macrophages derived from Ly6C(high) monocytes. Cancer Res. *70*, 5728–5739.

Palmer, C., Diehn, M., Alizadeh, A.A., and Brown, P.O. (2006). Cell-type specific gene expression profiles of leukocytes in human peripheral blood. BMC Genomics *7*, 115.

Ries, C.H., Cannarile, M.A., Hoves, S., Benz, J., Wartha, K., Runza, V., Rey-Giraud, F., Pradel, L.P., Feuerhake, F., Klaman, I., et al. (2014). Targeting tumor-associated macrophages with anti-CSF-1R antibody reveals a strategy for cancer therapy. Cancer Cell *25*, 846–859.

Savina, A., Jancic, C., Hugues, S., Guermonprez, P., Vargas, P., Moura, I.C., Lennon-Duménil, A.M., Seabra, M.C., Raposo, G., and Amigorena, S. (2006). NOX2 controls phagosomal pH to regulate antigen processing during crosspresentation by dendritic cells. Cell *126*, 205–218.

Schulz, C., Gomez Perdiguero, E., Chorro, L., Szabo-Rogers, H., Cagnard, N., Kierdorf, K., Prinz, M., Wu, B., Jacobsen, S.E., Pollard, J.W., et al. (2012). A lineage of myeloid cells independent of Myb and hematopoietic stem cells. Science *336*, 86–90.

Strachan, D.C., Ruffell, B., Oei, Y., Bissell, M.J., Coussens, L.M., Pryer, N., and Daniel, D. (2013). CSF1R inhibition delays cervical and mammary tumor growth in murine models by attenuating the turnover of tumor-associated macrophages and enhancing infiltration by CD8(+) T cells. OncoImmunology *2*, e26968.

Tamura, T., Tailor, P., Yamaoka, K., Kong, H.J., Tsujimura, H., O'Shea, J.J., Singh, H., and Ozato, K. (2005). IFN regulatory factor-4 and -8 govern dendritic cell subset development and their functional diversity. J. Immunol. *174*, 2573–2581.

Viigimaa, M., Vaverkova, H., Farnier, M., Averna, M., Missault, L., Hanson, M.E., Dong, Q., Shah, A., and Brudi, P. (2010). Ezetimibe/simvastatin 10/20 mg versus rosuvastatin 10 mg in high-risk hypercholesterolemic patients stratified by prior statin treatment potency. Lipids Health Dis. *9*, 127.

Weinstein, J.N., Collisson, E.A., Mills, G.B., Shaw, K.R., Ozenberger, B.A., Ellrott, K., Shmulevich, I., Sander, C., and Stuart, J.M.; Cancer Genome Atlas Research Network (2013). The Cancer Genome Atlas Pan-Cancer analysis project. Nat. Genet. *45*, 1113–1120.

Williams, J.W., Tjota, M.Y., Clay, B.S., Vander Lugt, B., Bandukwala, H.S., Hrusch, C.L., Decker, D.C., Blaine, K.M., Fixsen, B.R., Singh, H., et al. (2013). Transcription factor IRF4 drives dendritic cells to promote Th2 differentiation. Nat. Commun. *4*, 2990.

Wolf, D.M., Lenburg, M.E., Yau, C., Boudreau, A., and van 't Veer, L.J. (2014). Gene co-expression modules as clinically relevant hallmarks of breast cancer diversity. PLoS ONE *9*, e88309.

Wyckoff, J., Wang, W., Lin, E.Y., Wang, Y., Pixley, F., Stanley, E.R., Graf, T., Pollard, J.W., Segall, J., and Condeelis, J. (2004). A paracrine loop between tumor cells and macrophages is required for tumor cell migration in mammary tumors. Cancer Res. *64*, 7022–7029.